

Fig. S1: Sample locations. Georeferenced Landsat imagery with labelled sampling locations; C = core, B = bank, P = pit samples.

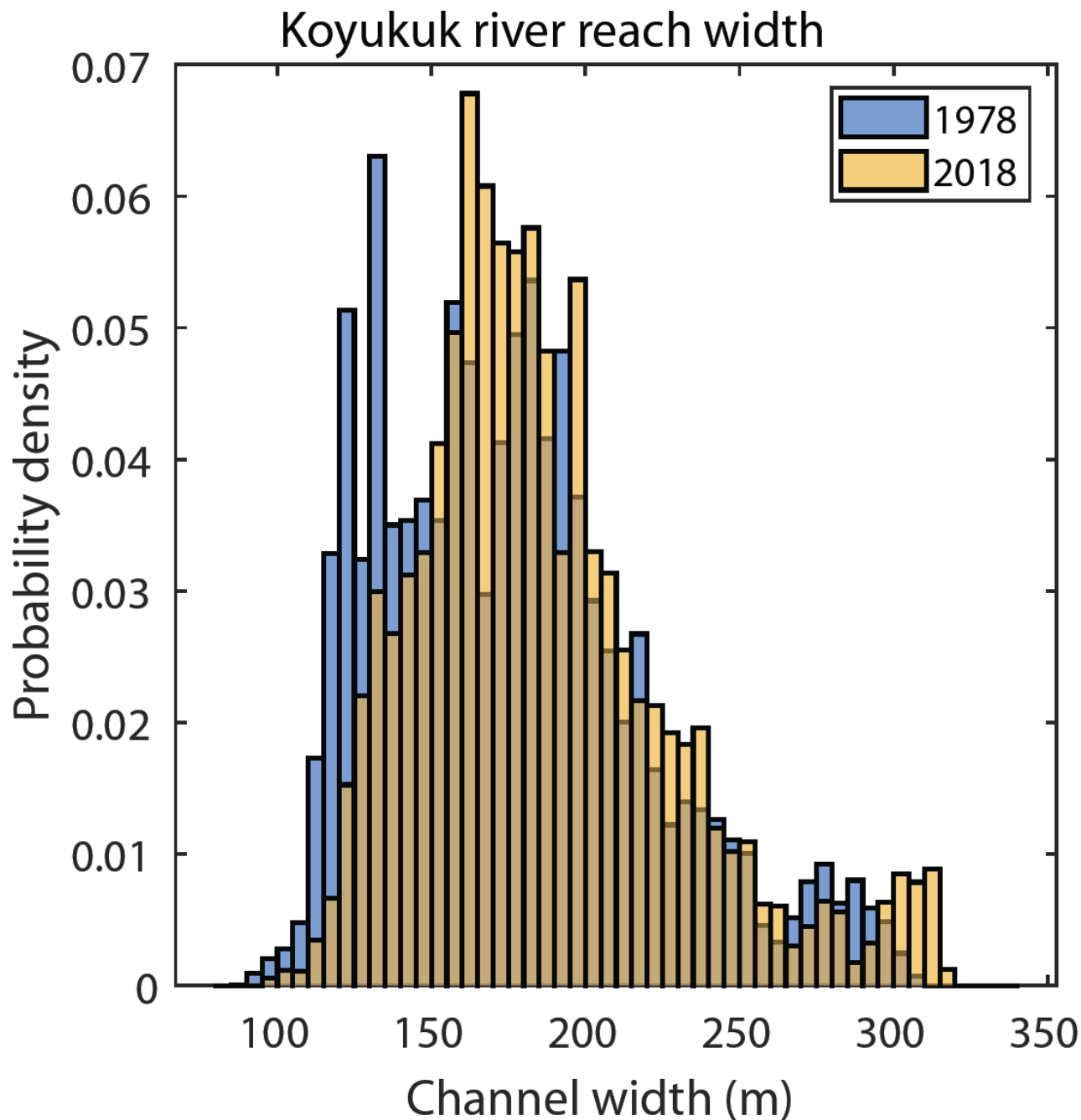
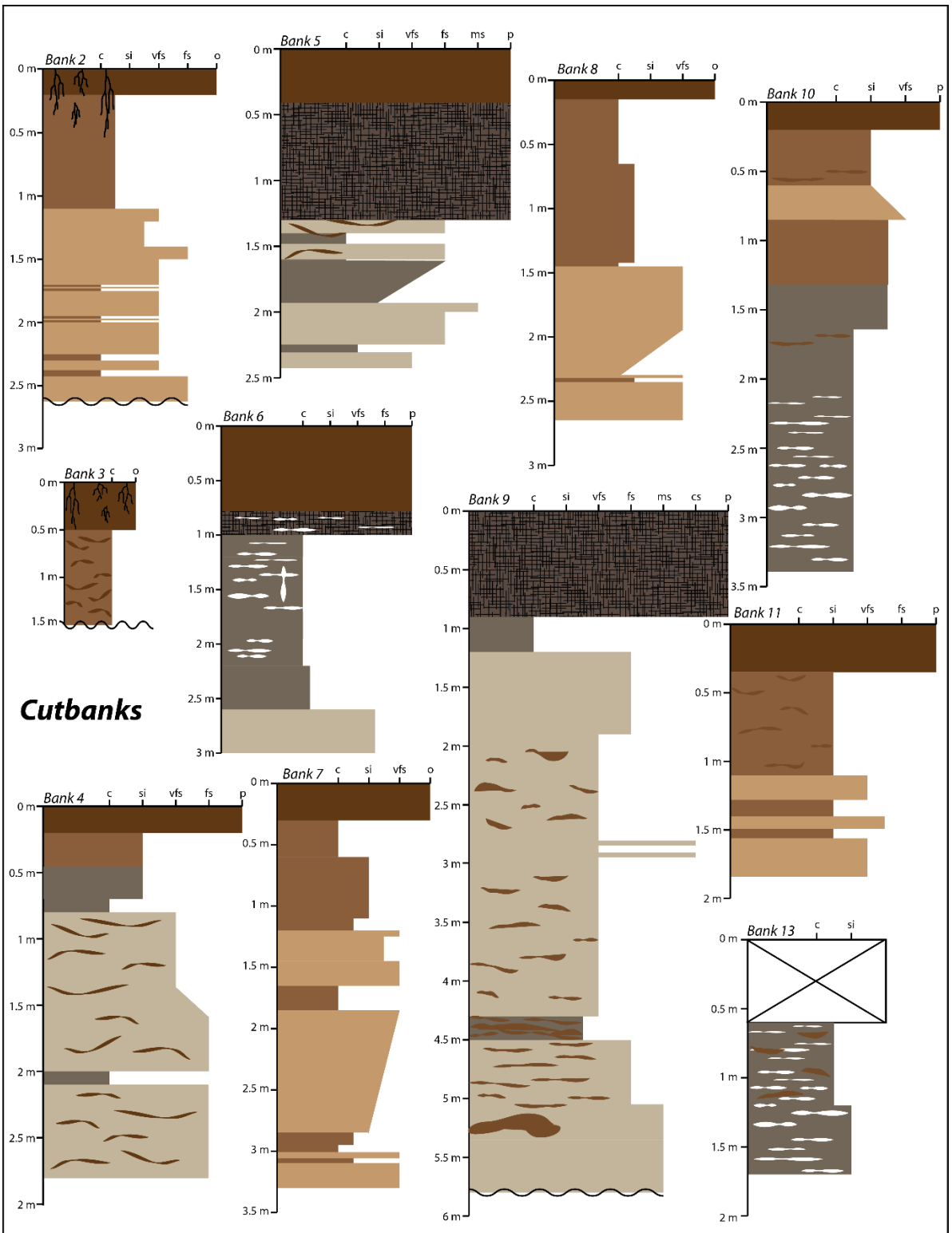
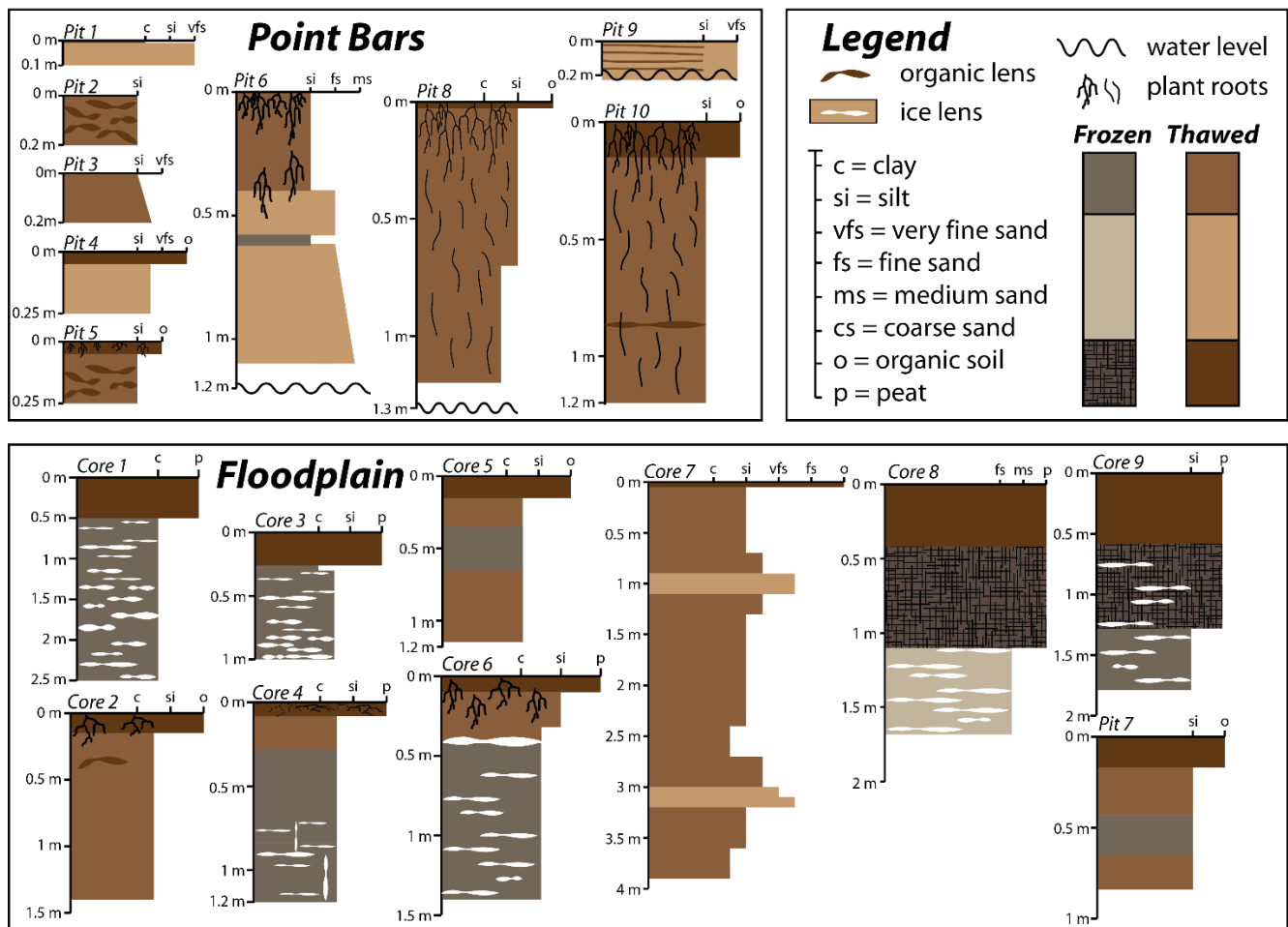


Fig. S2: Koyukuk River width. Probability distribution of width of channel masks generated from Landsat 30 m imagery, with widths calculated at each pixel along the channel centerline for the reach of the Koyukuk River pictured in Fig. S1 (Rowland et al., 2019). The reach maintained a roughly constant channel width over the Landsat record, from 173 ± 43 m (median \pm 1SD) in 1978 to 179 ± 42 m in 2018, supporting our assumption that cutbank erosion and point bar deposition occur at the same rate.





10 Fig. S3: Measured stratigraphic sections grouped by location on river floodplain. The river channel is eroding its cutbanks and depositing sediment on its point bars, which accrete to form the floodplain as the channel continues to migrate laterally. Note that deposits were generally sandy greater than 2 m depth below the floodplain surface, and that organic horizon thickness at the ground surface varies, though lenses of organic-rich sediment were prevalent meters below the surface. The active layer was shallower in permafrost units containing thick layers of peat, while locations without permafrost contained plant roots extending meters farther below the ground surface and lacked thermoerosional niches. Thicknesses of stratigraphic units were tabulated for each section in Table S4.

15

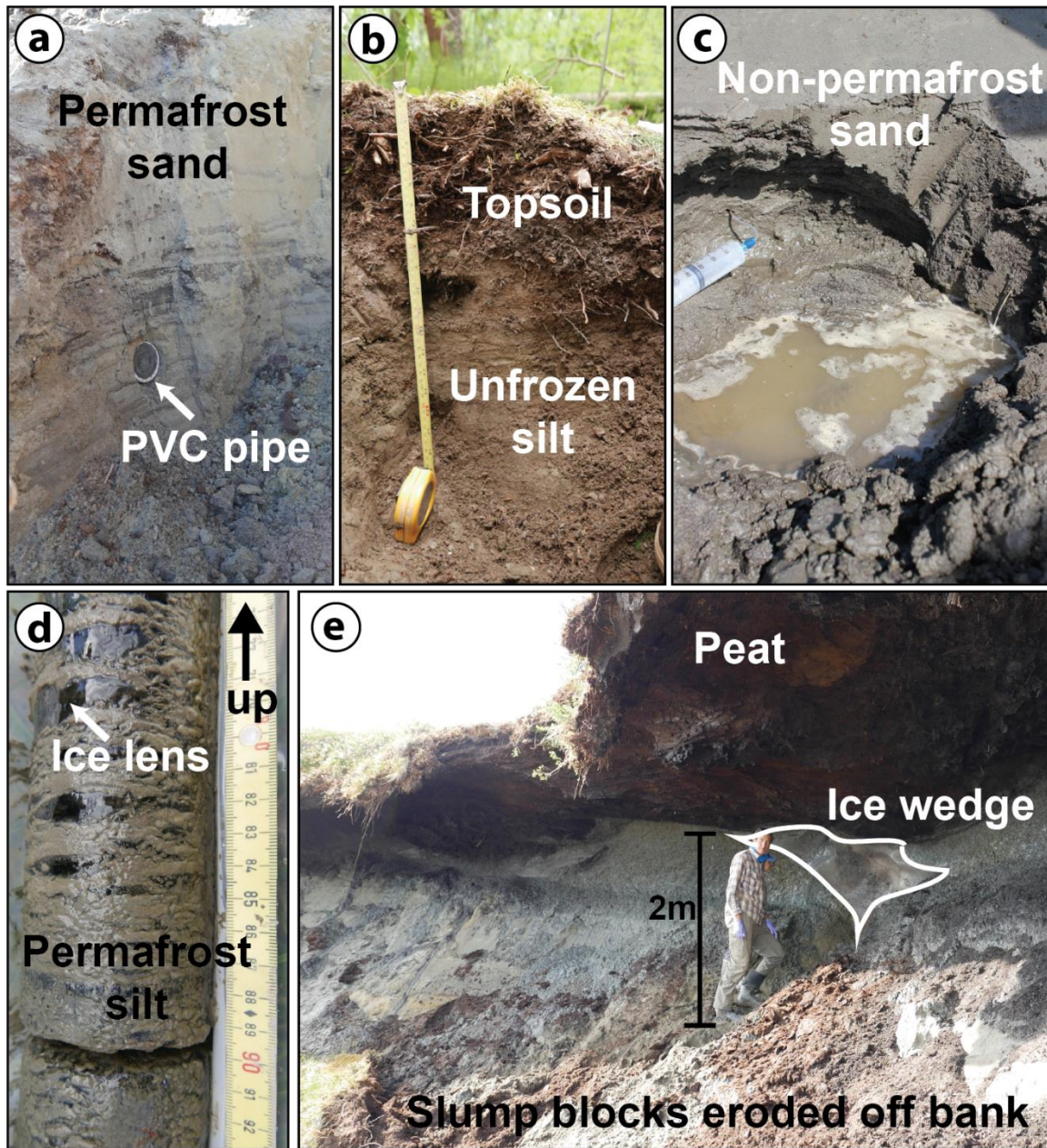


Fig. S4: Field photos of floodplain stratigraphic facies. (a) Permafrost sand in Bank 9 with 2 inch PVC pipe (outer diameter is 6.0 cm) installed in the bank for scale. (b) Pit dug in non-permafrost ground with root-rich topsoil overlying silt at Core 5. (c) Non-permafrost sandy deposits on a point bar beach at Pit 9. (d) Permafrost silt containing ice lenses in Core 4. (e) Overhung cutbank from Bank 9, with a layer of peat overlying an ice wedge surrounded by grey, frozen silt with slump blocks and intraclasts of thawed peat and silt forming a slope that shields the bank.

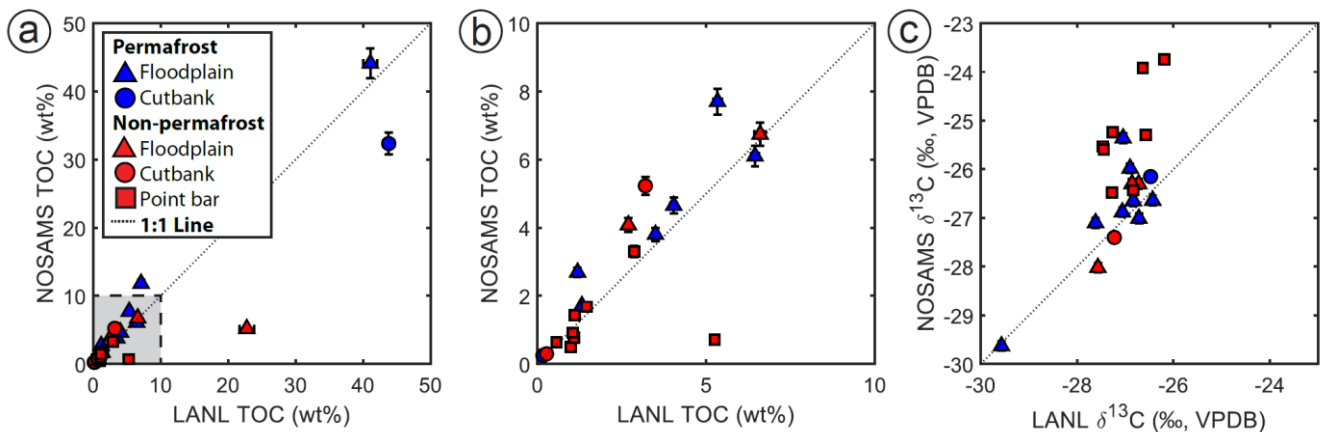


Fig. S5: Organic carbon measurement comparison, with samples with ^{13}C values $> -20\text{‰}$ excluded. TOC and OC stable isotopes were measured at both NOSAMS and Los Alamos National Lab (LANL), with NOSAMS generally showing a slightly higher TOC and $\delta^{13}\text{C}$. We attribute these differences to decarbonation procedures: using HCl in solution for the NOSAMS measurements and fumigation with HCl for the LANL measurements (see Sect. 3). All plots in the main text and supplemental materials use the LANL TOC and $\delta^{13}\text{C}$ values with NOSAMS radiocarbon measurements. (a) NOSAMS versus LANL TOC measurements, with error bars showing 1SD analytical uncertainty. (b) Zoomed in plot of shaded region in plot (a). (c) NOSAMS versus LANL OC stable isotope measurements, reported as per mille (‰) relative to VPDB with error bars showing 1SD analytical uncertainty.

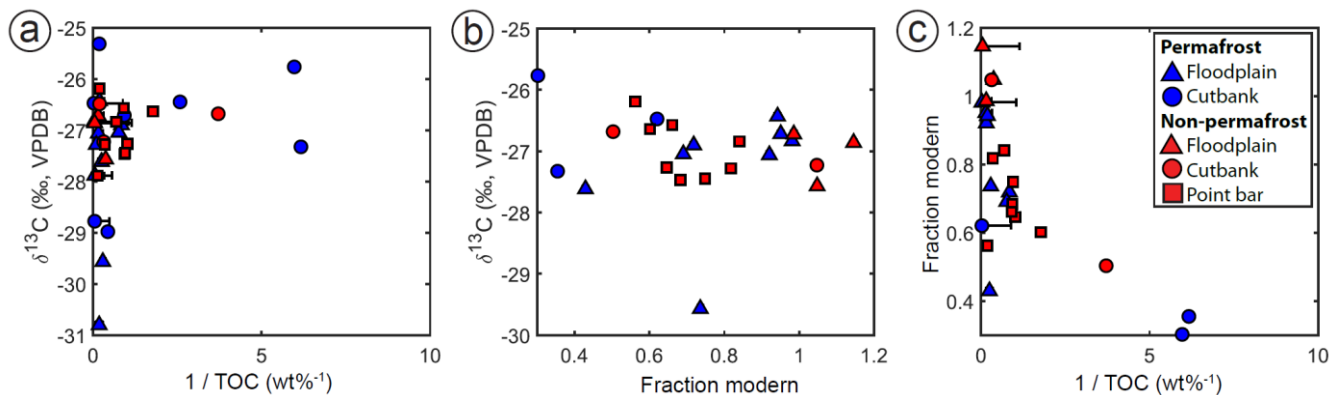


Fig. S6: Sediment OC characteristics, with samples with ^{13}C values $> -20\text{‰}$ excluded. Stable organic carbon isotopes displayed no trends with (a) inverse total organic carbon (TOC) or (b) radiocarbon fraction modern (Fm). Sediment $\delta^{13}\text{C}$ values spanned the range previously reported in peat and woody debris (from $-23.2 \pm 0.2 \text{‰}$ to $-28.6 \pm 0.2 \text{‰}$) on the Koyukuk River floodplain near its confluence with the Yukon River (O'Donnell et al., 2012). Stable organic carbon isotope values also incorporated a petrogenic end-member, and kerogen-rich sedimentary rocks in the Brooks Range had $\delta^{13}\text{C}$ ranging from $-27.23 \pm 0.1 \text{‰}$ to $-30.75 \pm 0.1 \text{‰}$ (Johnson et al., 2015). Measured $\delta^{13}\text{C}$ values are reported in units of per mille (‰) relative to the VPDB. (c) Fm decreased for high values of $1/\text{TOC}$ but spanned a wide range for low values of $1/\text{TOC}$, which we interpret as reflecting mixing between modern biospheric, aged biospheric, and petrogenic end-members. Sample x and y error bars show 1SD analytical uncertainty.

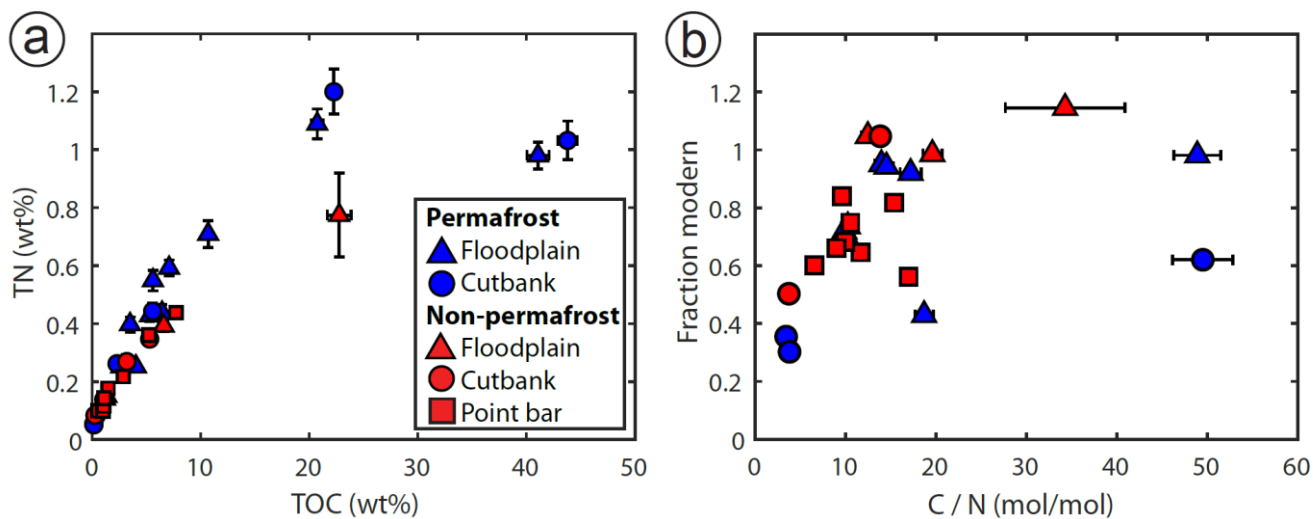


Fig. S7: Sediment total nitrogen. (a) Total nitrogen (TN) versus total organic carbon (TOC) measured as dry weight % of samples, with error bars showing 1SD analytical uncertainty. (b) Radiocarbon fraction modern values versus molar ratio of organic carbon to nitrogen, with error bars showing 1SD analytical uncertainty.

Sample site	Landform	Latitude (°)	Longitude (°)	Frozen ground type
Bank 1	Cutbank	65.78014	-156.43661	Permafrost
Bank 2	Cutbank	65.76493	-156.49031	Non-permafrost
Bank 3	Cutbank	65.76519	-156.48964	Non-permafrost
Bank 4	Cutbank	65.75232	-156.50511	Permafrost
Bank 5	Cutbank	65.75232	-156.50511	Permafrost
Bank 6	Cutbank	65.75232	-156.50511	Permafrost
Bank 7	Cutbank	65.66093	-156.45087	Non-permafrost
Bank 8	Cutbank	65.66126	-156.44711	Non-permafrost
Bank 9	Cutbank	65.70265	-156.40977	Permafrost
Bank 10	Cutbank	65.61942	-156.48534	Permafrost
Bank 11	Cutbank	65.62931	-156.46198	Non-permafrost
Bank 12	Cutbank	65.64022	-156.50949	Non-permafrost
Bank 13	Cutbank	65.87132	-156.26283	Permafrost
Bank 14	Cutbank	65.70153	-156.40353	Permafrost
Core 1	Floodplain	65.78014	-156.43661	Permafrost
Core 2	Floodplain	65.76521	-156.49049	Non-permafrost
Core 3	Floodplain	65.72090	-156.37178	Permafrost
Core 4	Floodplain	65.73519	-156.38866	Permafrost
Core 5	Floodplain	65.67904	-156.61163	Non-permafrost
Core 6	Floodplain	65.67158	-156.58762	Permafrost
Core 7	Point bar	65.66046	-156.43256	Non-permafrost
Core 8	Floodplain	65.72552	-156.20992	Permafrost
Core 9	Floodplain	65.71100	-156.27473	Permafrost
Pit 1	Point bar	65.77817	-156.43370	Non-permafrost
Pit 2	Point bar	65.77764	-156.43364	Non-permafrost
Pit 3	Point bar	65.77688	-156.43394	Non-permafrost
Pit 4	Point bar	65.77636	-156.43342	Non-permafrost
Pit 5	Point bar	65.77483	-156.43354	Non-permafrost
Pit 6	Point bar	65.77756	-156.43381	Non-permafrost
Pit 7	Floodplain	65.72083	-156.37217	Non-permafrost
Pit 8	Point bar	65.65986	-156.43524	Non-permafrost

Pit 9	Point bar	65.65958	-156.43542	Non-permafrost
Pit 10	Point bar	65.66132	-156.43354	Non-permafrost

Table S2: Sample descriptions and results of laboratory analysis. Starred samples have median grain size (D₅₀), TOC, TN, δ¹³C and molar TOC/TN ratios previously reported in Douglas et al. (2021).

Attached as file TableS2.csv

50

Table S3: Averaged sediment TOC concentrations and constants used in calculations of bank TOC content integrated to channel depth.

	Sand	Silt	Peat	Topsoil
D₅₀ (mm)	>0.063	<0.063	N/A	N/A
Water content (wt%)	18.1±6.1	46.6±15.6	87.5±7.4	62.2±1.0
TOC (wt%)	0.94±0.95	3.69±2.25	35.20±12.60	15.25±10.62
TOC (kgC/m³)	7.49±8.27	19.1±14.4	42.7±20.0	55.9±42.2
Bulk density (kg/m³)	971±283			
Channel Depth (m)	12.4			
Migration Rate (m/yr)	0.52			

Table S4: Calculation of bank TOC content integrated to channel depth based on measured stratigraphic columns. Note that unmeasured section was assumed to consist of sand based on field observations.

55 Attached as file TableS4.csv

Table S5: Complete grain size distributions measured using laser diffraction tabulated in log-normal bins, with 10th-, 50th- and 90th-percentile grain size reported as D₁₀, D₅₀, and D₉₀.

Attached as file TableS5.csv

60